# Chapter 13
# A Rubin-Based Reduced Order Model for Mistuned Bladed Disks: A Physically Interpretable and Experimentally Compatible Approach

**Umidjon Usmanov, Giuseppe Battiato, and Christian Maria Firrone**

**Abstract** The dynamic design of bladed disks is typically carried out under the assumption of ideal cyclic symmetry. In practice, however, manufacturing tolerances and assembly operations unavoidably introduce deviations in both stiffness and mass of each sector from their nominal values. This results in a mistuned assembly, which can lead to significantly higher blade vibration levels compared to the nominally tuned disk. Although full finite element (FE) models can be used to predict the response of mistuned bladed disks, the highly refined meshes employed by the designers in commercial FE software often make such analyses computationally expensive, sometimes even at the single-sector level under cyclic symmetry conditions. For this reason, the use of reduced-order models (ROMs) remains an effective strategy to enable feasible dynamic analyses for large-scale FE models. Traditionally, ROMs for mistuned bladed disks are based on fixed-interface methods. However, when the model must incorporate experimentally measured free-vibration modes of the blades, as well as the actual contact conditions between blades and disk slots, fixed-interface methods become limited. This is because they rely on perturbing the eigenvalues of fixed-interface normal modes, which require strong assumptions about the interface constraints—assumptions that may differ significantly from the real contact conditions. In this work, a novel ROM method for mistuned bladed disks is proposed, based on the Rubin method, which belongs to the class of free-interface methods. This formulation allows the use of free–free blade modes, which can be reliably measured experimentally and are independent of blade–disk boundary conditions. The resulting model provides a simpler, more robust, and physically meaningful framework for the prediction of mistuned bladed-disk dynamics. Comparisons with full FE models demonstrate that the proposed method is straightforward to implement, physically interpretable, and capable of accurately capturing both small and large mistuning.

**Keywords** Bladed disks, Mistuning, Reduced Order Models, Free interface reduction, vibration analysis

## Introduction

The dynamic response of turbine blades is highly sensitive to small deviations in their properties, making mistuning an unavoidable challenge in bladed disk design. Such deviations may arise from manufacturing tolerances, material variations, or in-service wear, and even small differences can lead to substantial amplification of vibration amplitudes [1]. This amplification not only increases the risk of high-cycle fatigue but also complicates the prediction of system response, since certain blades may experience localized vibration energy far above the levels expected in an ideal tuned system.

To investigate mistuning effects, many studies have employed simplified lumped-parameter models that treat the bladed disk as a set of coupled mass-spring systems [2, 3]. While these models provide valuable physical insight and allow efficient parametric studies, their accuracy is often insufficient for capturing the true behavior of real bladed disks. On the other hand, finite element (FE) models provide a higher level of fidelity but require significant computational resources, particularly for mistuned bladed disks, where mistuning patterns arise from geometric or material variations across the blades in the assembly. As a result, even the evaluation of the linear mistuned response becomes cumbersome due to the high computational

Umidjon Usmanov · Giuseppe Battiato · Christian Maria Firrone
Department of Mechanical and Aerospace Engineering
Polytechnic University of Turin, Turin, Italy 10129
e-mail: umidjon.usmanov@polito.it; giuseppe.battiato@polito.it; christian.firrone@polito.it

© The Author(s), under exclusive license to River Publishers 2026

Kristin B. Zimmerman, PhD (eds.), *Dynamic Substructuring & Transfer Path Analysis, 2026, Vol. 4*, Conference Proceedings of the Society for Experimental Mechanics Series, https://doi.org/10.13052/rp-9788743814153

cost of dynamic analyses, and capturing the global behavior of the mistuned assembly often becomes prohibitive, as it typically requires simulating several mistuning patterns. This trade-off highlights the need for advanced reduced order modeling (ROM) strategies that combine physical accuracy with computational efficiency.

Over the past decades, the problem of mistuning in bladed disks has been the subject of extensive research. Numerous modeling strategies have been proposed to balance accuracy and computational cost, ranging from simplified lumped-parameter models to advanced finite-element-based reduced order models. In [4], Yang and Griffin proposed a system level approach in which the mistuned system mode shapes are represented as a linear combination of tuned modes, specifically a subset of nominal system modes (SNM). Bladh et al. proposed a component level approach in which the mistuning is confined to individual component (superelements), namely component mode based reduced order modeling technique, widely known as CMM method [5–6]. In this work, the authors proposed an efficient method to introduce a mistuning pattern into the ROM of a blisk by perturbing the natural frequencies of the fixed-interface (i.e., cantilever) blades, which explicitly appear in the reduced stiffness matrix. Feiner and Griffin extended the SNM method presented in [4] by simplifying the formulation when the nominal modes used in the representation are limited to a single modal family [7]. This approach is known as Fundamental Model of Mistuning (FMM). Vargiu et al. extended the CMM method, making it suitable not only when mistuning is confined to the blades but also when it affects the disk, or when blades cannot be removed from the assembly, as in the case of blisks [8]. Pourkiaee and Zucca developed a reduced order model for nonlinear vibration analysis of mistuned bladed disks with shrouds. This was achieved by employing component mode synthesis method followed by modal synthesis based on loaded interface mode shapes [9]. In [10], Saletti et al. proposed a further mistuned ROM for the nonlinear forced-response analysis of bladed disks with localized contact nonlinearities.

This paper presents a novel method for mistuned bladed disks reduction based on the method developed by Rubin [11]. The proposed approach, referred to as the Free-Interface Blade Mistuning (FIBM) method, allows to model the mistuning pattern in the bladed disk ROM by perturbating the natural frequencies associated to the free–free normal modes of the blade. Such modes have the advantage that can be reliably identified from experimental tests performed under free-free conditions, a well-established practice in experimental modal analysis, making the method suitable for replicating real mistuning patterns. Moreover, the FIBM method enables the retention of arbitrary sets of active DOFs in the ROM without compromising either the physical interpretability of the reduced model or the accuracy of the applied mistuning pattern.

## Methodology

This section presents the FIBM method for the reduction of a FE mistuned bladed disk. First, starting from a single sector of the FE model, which includes the fundamental disk sector and the nominal blade, a strategy for partitioning the DOFs is provided, facilitating the application of subsequent reduction procedures. Then, the reduction of the two FE substructures is carried out separately, using the Craig–Bampton method [12] for the disk sector and the Rubin method [11] for the nominal blade. Finally, the modeling strategy adopted to obtain the assembled ROM of the bladed disk, as well as the procedure through which blade mistuning patterns are incorporated into it, is presented and discussed.

A bladed disk is nominally a cyclic structure composed of N identical sectors, each consisting of two substructures, i.e., the disk sector and the blade (Figure 1). With reference to the substructures highlighted in green in Figure 1, the vectors of DOFs for the disk sector and blade can be partitioned as follows:

$$\boldsymbol{x}^D = \begin{Bmatrix} \boldsymbol{x}_i^D \\ \boldsymbol{x}_l^D \\ \boldsymbol{x}_h^D \\ \boldsymbol{x}_e^D \end{Bmatrix}, \qquad \boldsymbol{x}^B = \begin{Bmatrix} \boldsymbol{x}_i^B \\ \boldsymbol{x}_a^B \\ \boldsymbol{x}_e^B \end{Bmatrix} \tag{1}$$

In this notation, the superscripts $D$ and $B$ denote the DOFs associated with the disk sector and the blade, respectively. The subscript $i$ in both vectors refers to the DOFs located at the blade root joint *interface*, i.e., the contact region between the blade and the corresponding slot in the disk (Figure 1). For the disk sector, the subscripts $l$ and $h$ indicated the DOFs at the *low* and *high* frontier of the sector. For the blade, the subscript $a$ identifies the *accessory* DOFs, i.e., DOFs not directly involved in the interface or structural coupling. Finally, the partitions denoted by the subscript $e$ in both vectors refer to the *exceeding* DOFs, i.e., those which are not retained as master in the corresponding reduction procedures. Note that each subscript also implicitly defines the size of the corresponding partition: for example, the subscript $i$ in $\boldsymbol{x}_i^D$ denotes that vector is of size $n_i^D$.

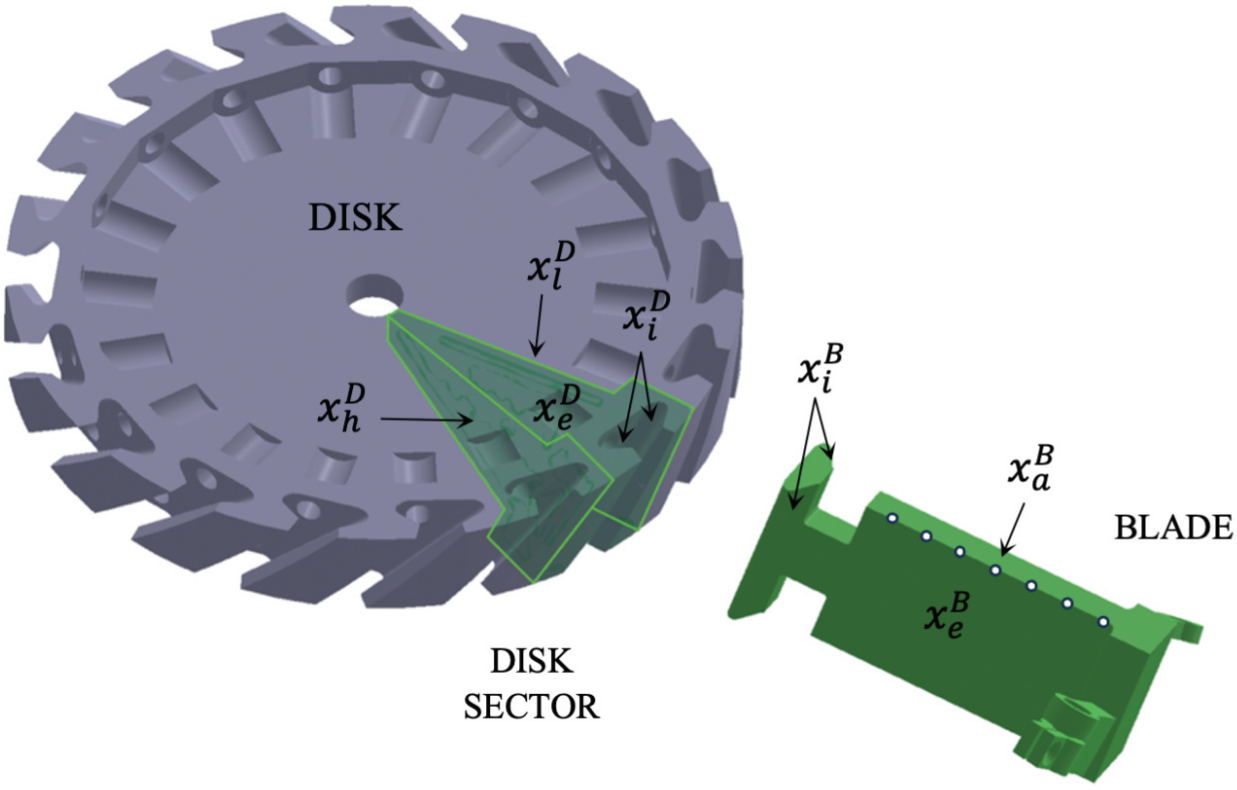


**Fig. 1** Schematic representation of the bladed-disk system showing the disk sector and blade component with the definition of boundary, interface, and auxiliary degrees of freedom

Given the partitioning defined in Eq. (1), the FE mass and stiffness matrices for the disk sector and blade can be written as:

$$\boldsymbol{M}^D = \begin{bmatrix} \boldsymbol{M}^D_{\mathrm{ii}} & \boldsymbol{M}^D_{il} & \boldsymbol{M}^D_{ih} & \boldsymbol{M}^D_{ie} \\ \boldsymbol{M}^D_{li} & \boldsymbol{M}^D_{ll} & \boldsymbol{M}^D_{lh} & \boldsymbol{M}^D_{le} \\ \boldsymbol{M}^D_{hi} & \boldsymbol{M}^D_{hl} & \boldsymbol{M}^D_{hh} & \boldsymbol{M}^D_{he} \\ \boldsymbol{M}^D_{ei} & \boldsymbol{M}^D_{el} & \boldsymbol{M}^D_{eh} & \boldsymbol{M}^D_{ee} \end{bmatrix} \quad \boldsymbol{K}^D = \begin{bmatrix} \boldsymbol{K}^D_{\mathrm{ii}} & \boldsymbol{K}^D_{il} & \boldsymbol{K}^D_{ih} & \boldsymbol{K}^D_{ie} \\ \boldsymbol{K}^D_{li} & \boldsymbol{K}^D_{ll} & \boldsymbol{K}^D_{lh} & \boldsymbol{K}^D_{le} \\ \boldsymbol{K}^D_{hi} & \boldsymbol{K}^D_{hl} & \boldsymbol{K}^D_{hh} & \boldsymbol{K}^D_{he} \\ \boldsymbol{K}^D_{ei} & \boldsymbol{K}^D_{el} & \boldsymbol{K}^D_{eh} & \boldsymbol{K}^D_{ee} \end{bmatrix} \tag{2}$$

$$\boldsymbol{M}^B = \begin{bmatrix} \boldsymbol{M}^B_{\mathrm{ii}} & \boldsymbol{M}^B_{ia} & \boldsymbol{M}^B_{ie} \\ \boldsymbol{M}^B_{ai} & \boldsymbol{M}^B_{aa} & \boldsymbol{M}^B_{ae} \\ \boldsymbol{M}^B_{ei} & \boldsymbol{M}^B_{ea} & \boldsymbol{M}^B_{ee} \end{bmatrix} \quad \boldsymbol{K}^B = \begin{bmatrix} \boldsymbol{K}^B_{\mathrm{ii}} & \boldsymbol{K}^B_{ia} & \boldsymbol{K}^B_{ie} \\ \boldsymbol{K}^B_{ai} & \boldsymbol{K}^B_{aa} & \boldsymbol{K}^B_{ae} \\ \boldsymbol{K}^B_{ei} & \boldsymbol{K}^B_{ea} & \boldsymbol{K}^B_{ee} \end{bmatrix} \tag{3}$$

To enable reduction of both substructures, the non-exceeding DOFs can be conveniently grouped into the following vectors of *boundary* DOFs:

$$\boldsymbol{x}^D_b = \begin{Bmatrix} \boldsymbol{x}^D_i \\ \boldsymbol{x}^D_l \\ \boldsymbol{x}^D_h \end{Bmatrix}, \qquad \boldsymbol{x}^B_b = \begin{Bmatrix} \boldsymbol{x}^B_i \\ \boldsymbol{x}^B_a \end{Bmatrix} \tag{4}$$

Considering the DOFs partitioning defined in Eq. (1) and Eq. (4), the mass and stiffness FE matrices of Eqs. (2) and (3) can be expressed in a more compact form as:

$$\boldsymbol{M}^D = \begin{bmatrix} \boldsymbol{M}^D_{bb} & \boldsymbol{M}^D_{be} \\ \boldsymbol{M}^D_{eb} & \boldsymbol{M}^D_{ee} \end{bmatrix} \quad \boldsymbol{K}^D = \begin{bmatrix} \boldsymbol{K}^D_{bb} & \boldsymbol{K}^D_{be} \\ \boldsymbol{K}^D_{eb} & \boldsymbol{K}^D_{ee} \end{bmatrix} \tag{5}$$

$$\boldsymbol{M}^B = \begin{bmatrix} \boldsymbol{M}^B_{bb} & \boldsymbol{M}^B_{be} \\ \boldsymbol{M}^B_{eb} & \boldsymbol{M}^B_{ee} \end{bmatrix} \quad \boldsymbol{K}^B = \begin{bmatrix} \boldsymbol{K}^B_{bb} & \boldsymbol{K}^B_{be} \\ \boldsymbol{K}^B_{eb} & \boldsymbol{K}^B_{ee} \end{bmatrix} \tag{6}$$

The disk sector is reduced using the Craig–Bampton (HCB) method [12], according to which the displacement field associated with the exceeding DOFs is expressed as a linear combination of two sets of component modes. The first set,

referred to as *Constraint (or static) modes* and denoted by $\boldsymbol{\Psi}_{eb}$, represents the matrix of static displacements at the exceeding DOFs, where each column corresponds to the deformation resulting from the application of a unit displacement at a given boundary DOF while all the others are held fixed. The second set, denoted by $\boldsymbol{\Phi}_{ek}$, collects a reduced set of $n_k$ (with $n_k \ll n_e^D$) of *Fixed-Interface normal modes*, which capture the dynamic flexibility of the substructure under the assumption that the set $\boldsymbol{x}_b^D$ is fully constrained. Such modes are obtained by solving the eigenvalue problem associated with the matrices $\boldsymbol{M}_{ee}^D$ and $\boldsymbol{K}_{ee}^D$. The application of the CB method leads to the following approximation of the physical displacement vector $\boldsymbol{x}^D$

$$\boldsymbol{x}^D = \left\{ \begin{array}{c} \boldsymbol{x}_b^D \\ \boldsymbol{x}_e^D \end{array} \right\} \approx \left[ \begin{array}{cc} \boldsymbol{I}_{bb} & \boldsymbol{0}_{bk} \\ \boldsymbol{\Psi}_{eb} & \boldsymbol{\Phi}_{ek} \end{array} \right] \left\{ \begin{array}{c} \boldsymbol{x}_b^D \\ \boldsymbol{\eta}_k^D \end{array} \right\} = \boldsymbol{R}_{CB}^D \, \boldsymbol{q}_{CB}^D \tag{7}$$

where $\boldsymbol{R}_{CB}^D$ is the CB reduction matrix, and $\boldsymbol{\eta}_k^D$ is the vector of modal amplitudes associated to the retained Fixed-Interface Normal modes. The vector $\boldsymbol{q}_{CB}^D = \left\{ (\boldsymbol{x}_b^D)^T \, (\boldsymbol{\eta}_k^D)^T \right\}^T$ thus represents the reduced generalized coordinate vector in the CB formulation.

When the number of DOFs at the disk sector frontiers is large, an additional reduction is often required to make further operations on the disk sector ROM more efficient and less time-consuming [13, 14]. A suitable approach for achieving a more compact representation of the frontier displacements is the *Gram-Schmidt Interface (GSI) reduction method* [17, 18]. According to this method, a selected subset of boundary DOFs can be further processed and approximated using a basis of orthonormal GSI modes. In particular, for the disk sector, the physical displacement partitions $\boldsymbol{x}_l^D$ and $\boldsymbol{x}_h^D$ can be approximated as:

$$\boldsymbol{x}_l^D \approx \boldsymbol{\Theta}_{lw_1} \eta_l^d \, , \; \boldsymbol{x}_h^D \approx \boldsymbol{\Theta}_{hw_2} \eta_h^D \tag{8}$$

where $\boldsymbol{\Theta}_{lw_1}$ and $\boldsymbol{\Theta}_{hw_2}$ are the truncated sets of GSI modes, while $\boldsymbol{\eta}_l^D$ and $\boldsymbol{\eta}_h^D$ are the corresponding reduced vectors of GSI modal coordinates. Assuming that the FE mesh is identical at both frontiers of the disk sector, the displacement vectors $\boldsymbol{x}_l^D$ and $\boldsymbol{x}_h^D$ have the same size (i.e., $n_l = n_h$). A common subset of $n_w$ GSI modes can therefore be defined to reduce both $\boldsymbol{x}_l^D$ and $\boldsymbol{x}_h^D$ using the following coordinate transformations:

$$\boldsymbol{x}_l^D \approx \boldsymbol{\Theta}_{lw} \eta_l^D \, , \; \boldsymbol{x}_h^D \approx \boldsymbol{\Theta}_{lw} \eta_h^D \tag{9}$$

Using Eq. (9), the Craig–Bampton generalized coordinate vector introduced in Eq. (7) can be further reduced as:

$$\left\{ \begin{array}{c} \boldsymbol{x}_i^D \\ \boldsymbol{x}_l^D \\ \boldsymbol{x}_h^D \\ \boldsymbol{\eta}_k^D \end{array} \right\} \approx \left[ \begin{array}{cccc} \boldsymbol{I_i} & \boldsymbol{0} & \boldsymbol{0} & \boldsymbol{0} \\ \boldsymbol{0} & \boldsymbol{\Theta}_{lw} & \boldsymbol{0} & \boldsymbol{0} \\ \boldsymbol{0} & \boldsymbol{0} & \boldsymbol{\Theta}_{lw} & \boldsymbol{0} \\ \boldsymbol{0} & \boldsymbol{0} & \boldsymbol{0} & \boldsymbol{I_k} \end{array} \right] \left\{ \begin{array}{c} \boldsymbol{x}_i^D \\ \boldsymbol{\eta}_l^D \\ \boldsymbol{\eta}_h^D \\ \boldsymbol{\eta}_k^D \end{array} \right\} = \boldsymbol{R}_{GSI}^D \boldsymbol{q}_{GSI}^D \tag{10}$$

where $\boldsymbol{R}_{\boldsymbol{GSI}}^{\boldsymbol{D}}$ is the GSI global reduction matrix, and $\boldsymbol{q}_{GSI}^D = \left\{ (\boldsymbol{x}_i^D)^T \, (\boldsymbol{\eta}_l^D)^T \, (\boldsymbol{\eta}_l^D)^T \, (\boldsymbol{\eta}_k^D)^T \right\}^T$ thus represents the reduced generalized coordinate vector in the GSI formulation.

Finally, the reduced mass and stiffness matrices of the disk sector can be obtained by the following coordinate transformation and projections:

$$\boldsymbol{M}_{red}^D = \left( \boldsymbol{R}_{CB}^D \, \boldsymbol{R}_{GSI}^D \right)^T \boldsymbol{M}^D \left( \boldsymbol{R}_{CB}^D \, \boldsymbol{R}_{GSI}^D \right); \qquad \boldsymbol{K}_{red}^D = \left( \boldsymbol{R}_{CB}^D \, \boldsymbol{R}_{GSI}^D \right)^T \boldsymbol{K}^D \left( \boldsymbol{R}_{CB}^D \, \boldsymbol{R}_{GSI}^D \right) \tag{11}$$

Once the ROM of the disk sector is obtained, the assembly of the disk can be performed in two alternative ways. One possibility is to use the disk representation used on the reduction method Component-Mode-Based ROM for mistuned bladed. disks (CMM) [6]. The other, used in this work, requires assembling the N ROMs defined by Eq. (11) by enforcing the compatibility of the GSI modal coordinates used to approximate the physical displacements at the disk frontiers. For two adjacent disk-sectors such condition can be expressed as:

$$^{(j-1)}\boldsymbol{\eta}_h^D = {}^{(j)}\boldsymbol{\eta}_l^D \tag{12}$$

Mathematically, the procedure is realized using a Boolean assembly matrix $\boldsymbol{A}^D$, which ensures that the displacements are equalized across neighboring sectors [19]:

$$\boldsymbol{M}_{full}^D = \left( \boldsymbol{A}^D \right)^T \left( \boldsymbol{I}_{NN} \otimes \boldsymbol{M}_{red}^D \right) \boldsymbol{A}^D; \qquad \boldsymbol{K}_{full}^D = \left( \boldsymbol{A}^D \right)^T \left( \boldsymbol{I}_{NN} \otimes \boldsymbol{K}_{red}^D \right) \boldsymbol{A}^D \tag{13}$$

The blade component is reduced using the Rubin method [11], which aims to represent the dynamic behavior of the substructure through a reduced basis consisting of its *free vibration modes* $\boldsymbol{\Phi}_f$, and the set of *residual attachment modes*

$\boldsymbol{\Psi}_r$. With reference to the boundary DOFs $\boldsymbol{x}_b^B$, each attachment mode corresponds to the static displacement response of the substructure when a unit force is applied at one DOF in $\boldsymbol{x}_b^B$, while all other DOFs remain force-free. One key advantage of the Rubin method over the CB method is that the free dynamic response of the substructure can be experimentally identified, for instance through modal testing in free–free boundary conditions. This eliminates the need to impose assumptions on interface constraints during testing, making the method particularly well-suited when the real boundary conditions at the coupling interface are unknown or variable.

Furthermore, if the component is free-floating or includes unconstrained rigid body motions, the reduction basis can also include the corresponding *rigid body modes* $\boldsymbol{\Phi}_r$. In the most general case, the vector of the blade can therefore be approximated as:

$$\boldsymbol{x}^B = \boldsymbol{\Phi}_r \boldsymbol{\eta}_r^B + \boldsymbol{\Phi}_f \boldsymbol{\eta}_f^B + \boldsymbol{\Psi}_r \boldsymbol{g}_b^B = \begin{bmatrix} \boldsymbol{\Phi}_r & \boldsymbol{\Phi}_f & \boldsymbol{\Psi}_r \end{bmatrix} \begin{Bmatrix} \boldsymbol{\eta}_r^B \\ \boldsymbol{\eta}_f^B \\ \boldsymbol{g}_b^B \end{Bmatrix} = \boldsymbol{R}_R^B \boldsymbol{q}_R^B \tag{14}$$

where $\boldsymbol{R}_R^B$ is the Rubin reduction matrix and $\boldsymbol{q}_R^B = \left\{ (\boldsymbol{\eta}_r^B)^T \, (\boldsymbol{\eta}_f^B)^T (\boldsymbol{g}_b^B)^T \right\}^T$ is the corresponding reduced generalized coordinate vector in the Rubin formulation. In this representation, containing $\boldsymbol{\eta}_r^B$ and $\boldsymbol{\eta}_f^B$ are the generalized coordinates associated with the rigid body and free-interface modes, respectively, while $\boldsymbol{g}_b^B$ contains the forces acting at the boundary DOFs.

By projecting the blade FE mass and stiffness matrices onto the space spanned by the columns of $\boldsymbol{R}_R^B$, the following reduced matrices are obtained:

$$\boldsymbol{M}_{red,1}^B = \begin{bmatrix} \boldsymbol{I_r} & \boldsymbol{0} & \boldsymbol{0} \\ \boldsymbol{0} & \boldsymbol{I_f} & \boldsymbol{0} \\ \boldsymbol{0} & \boldsymbol{0} & \boldsymbol{M}_{r,b}^B \end{bmatrix}; \quad \boldsymbol{K}_{red,1}^B = \begin{bmatrix} \boldsymbol{0} & \boldsymbol{0} & \boldsymbol{0} \\ \boldsymbol{0} & \boldsymbol{\Omega}_f^2 & \boldsymbol{0} \\ \boldsymbol{0} & \boldsymbol{0} & \boldsymbol{G}_{r,b}^B \end{bmatrix} \tag{15}$$

where $\boldsymbol{M}_{r,b}^B$ and $\boldsymbol{G}_{r,b}^B$ are the interface inertia associated to the residual flexibility modes, and the residual flexibility at the boundary, respectively. For further details on the computation of the block matrices $\boldsymbol{M}_{r,b}^B$ and $\boldsymbol{G}_{r,b}^B$, the reader is referred to [19].

From Eq. (15), it can be seen that the reduced stiffness matrix contains a diagonal block $\boldsymbol{\Omega}_f^2$, which includes the squared natural frequencies of the free–free modes of the blade. This block has a clear physical interpretation, as it directly characterizes the intrinsic dynamic behavior of the substructure, independently of any boundary conditions. Importantly, this interpretation does not depend on the choice of the boundary DOFs, in contrast to fixed-interface reduction methods such as CB, where the corresponding frequencies are tied to the boundary constraints imposed during modal extraction.

However, the reduction obtained using the Rubin method does not directly yield a standard super-element formulation, since the reduced coordinates include the interface forces $\boldsymbol{g}_b^B$ rather than interface displacements. To recover a form compatible with standard substructuring and global coupling procedures, the following secondary transformation must be applied [15]:

$$\begin{Bmatrix} \boldsymbol{\eta}_r^B \\ \boldsymbol{\eta}_f^B \\ \boldsymbol{g}_b^B \end{Bmatrix} = \begin{bmatrix} \boldsymbol{I_r} & \boldsymbol{0} & \boldsymbol{0} \\ \boldsymbol{0} & \boldsymbol{I_f} & \boldsymbol{0} \\ -\boldsymbol{G}_r^{-1} \boldsymbol{A} \boldsymbol{\Phi_r} & -\boldsymbol{G}_r^{-1} \boldsymbol{A} \boldsymbol{\Phi}_f & \boldsymbol{G}_r^{-1} \end{bmatrix} \begin{Bmatrix} \boldsymbol{\eta}_r^B \\ \boldsymbol{\eta}_f^B \\ \boldsymbol{x}_b^B \end{Bmatrix} = \boldsymbol{T}_2^B \begin{Bmatrix} \boldsymbol{\eta}_r^B \\ \boldsymbol{\eta}_f^B \\ \boldsymbol{x}_b^B \end{Bmatrix} \tag{16}$$

In this expression, $\boldsymbol{A}$ is the Boolean selection matrix used to extract the boundary DOFs from the full displacement vector, while $\boldsymbol{G}_r$ represent the residual flexibility corresponding to boundary DOFs, which is computed as:

$$\boldsymbol{G}_r = \boldsymbol{A} \cdot \boldsymbol{\Psi}_r \tag{17}$$

Through the successive application of the primary reduction (Rubin basis) and the secondary transformation $\boldsymbol{T}_2^B$, the final free-interface Rubin reduction matrix is obtained. The corresponding reduced mass and stiffness matrices for the blade component are then computed via congruent projection as:

$$\boldsymbol{M}_{red}^B = \left(\boldsymbol{T}_2^B\right)^T \boldsymbol{M}_{red,1}^B \left(\boldsymbol{T}_2^B\right); \qquad \boldsymbol{K}_{red}^B = \left(\boldsymbol{T}_2^B\right)^T \boldsymbol{K}_{red,1}^B \left(\boldsymbol{T}_2^B\right) \tag{18}$$

These matrices are now suitable for use in substructure coupling and assembly within the global ROM framework.

The final step consists in assembling the complete bladed-disk ROM. This is achieved by enforcing the compatibility condition between the disk and blade blade-root interface DOFs. Mathematically, the coupling is implemented through a Boolean assembly matrix $\boldsymbol{T}_{full}$, which ensures the continuity of displacements across the interfaces [16]. The global mass and stiffness matrices of the assembled system are thus given by:

$$\boldsymbol{M}_{full} = \boldsymbol{T}_{full}^T \begin{bmatrix} \boldsymbol{M}_{full}^D & \boldsymbol{0} \\ \boldsymbol{0} & \boldsymbol{I}_N \otimes \boldsymbol{M}_{red}^B \end{bmatrix} \boldsymbol{T}_{full}; \qquad \boldsymbol{K}_{full} = \boldsymbol{T}_{full}^T \begin{bmatrix} \boldsymbol{K}_{full}^D & \boldsymbol{0} \\ \boldsymbol{0} & \boldsymbol{I}_N \otimes \boldsymbol{K}_{red}^B \end{bmatrix} \boldsymbol{T}_{full}; \tag{19}$$

where $\boldsymbol{I}_N$ is the identity matrix of size equal to the number of blades, and $\otimes$ denotes the Kronecker product.

Assuming that the mode shapes of the blades in a mistuned bladed disk assembly do not differ significantly from those of the nominal blade, mistuning can be introduced at the blade level by perturbing the free-interface natural frequencies explicitly appearing in the diagonal block of the reduced stiffness matrix (see Eq. (15)). Since these frequencies are retained in the reduced-order model, they can be directly modified to account for blade-to-blade variations. This strategy offers significant flexibility, as each natural frequency associated with the free mode shape of any blade in the array can be individually adjusted. As a result, arbitrary mistuning patterns can be constructed in a straightforward and physically meaningful manner. The perturbed reduced stiffness matrix for a mistuned blade takes the form:

$$\boldsymbol{K}^{B}_{red,\ mist,1} = \begin{bmatrix} \mathbf{0} & \mathbf{0} & \mathbf{0} \\ \mathbf{0} & (\mathbf{1}+\boldsymbol{\chi}) \cdot \boldsymbol{\Omega}^2_f & \mathbf{0} \\ \mathbf{0} & \mathbf{0} & \boldsymbol{G}_{r,b} \end{bmatrix} \tag{20}$$

where $\boldsymbol{\chi}$ is a diagonal perturbation matrix defined as:

$$\boldsymbol{\chi} = \frac{\boldsymbol{\Omega}^2_{f,mist} - \boldsymbol{\Omega}^2_f}{\boldsymbol{\Omega}^2_f} \tag{21}$$

## Results

The proposed FIBM method was tested for the prediction of the natural frequencies of the academic mistuned bladed disk illustrated in Figure 2. The assembly consists of 18 sectors, all sharing the same geometry. Mistuning was introduced by assigning a different Young's modulus to each blade, while the disk sectors remained identical.

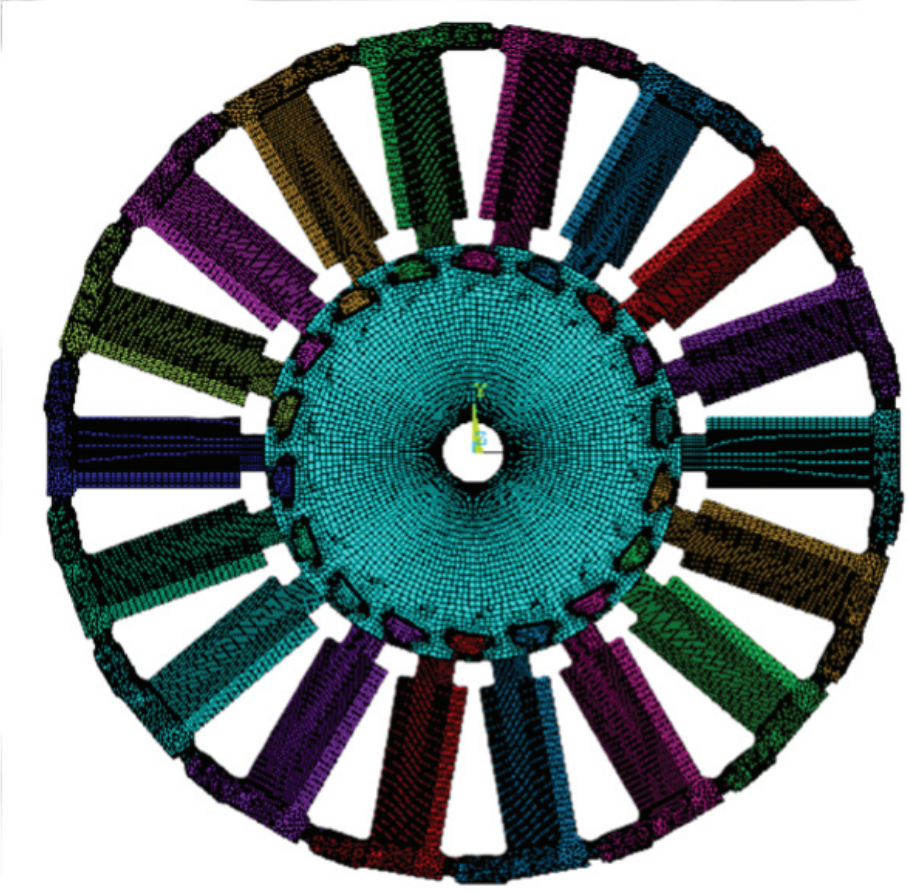

**Fig. 2** Mistuned full bladed disk assembly finite element model

The perturbation was generated by randomly sampling the Young's modulus of each blade from a normal distribution with a mean equal to that of the nominal blade (Figure 3).

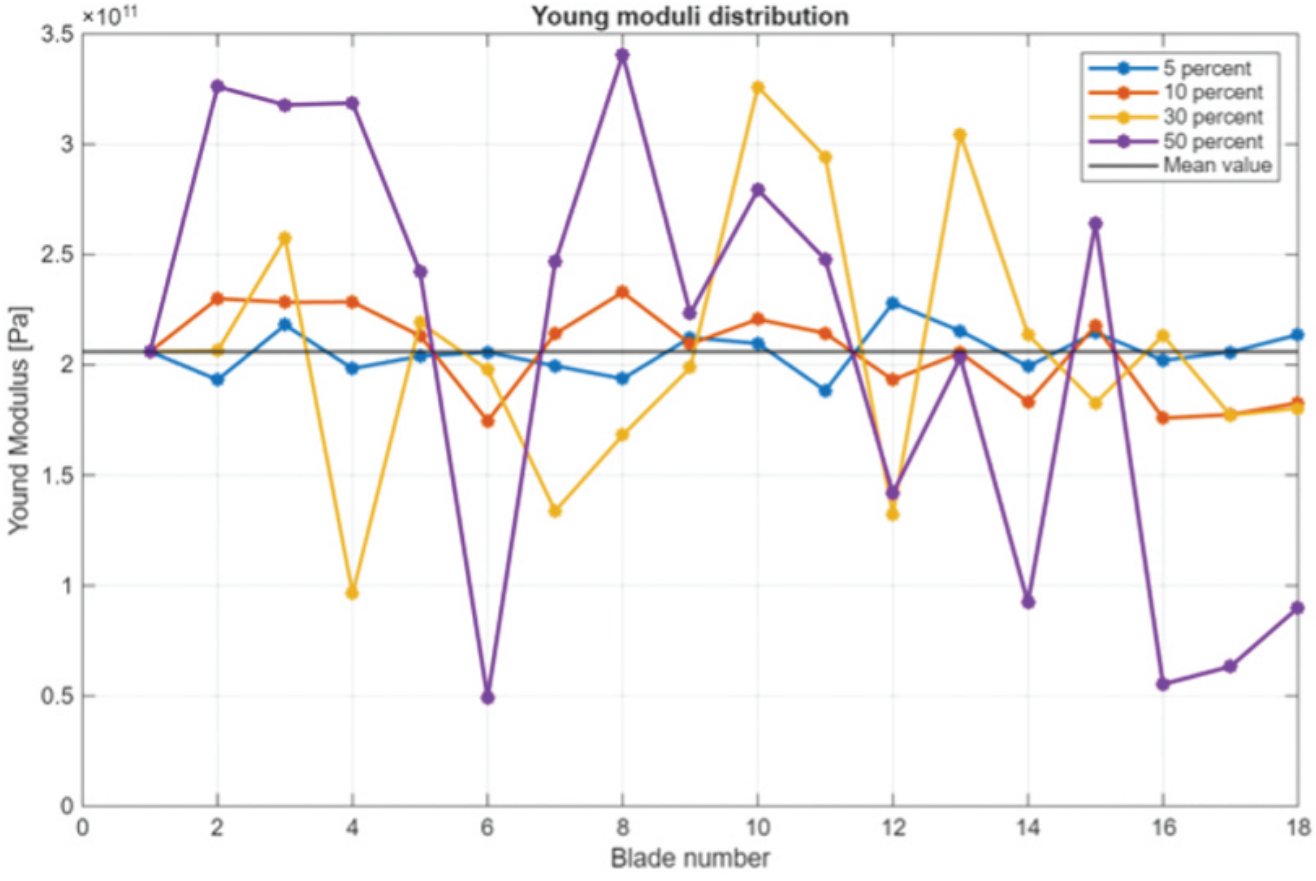


**Fig. 3** Distribution of the perturbed Young's modulus for the 18-blade assembly under different mistuning levels

To prevent any systematic drift from the nominal stiffness, the sample mean was adjusted to match the distribution mean. The resulting mistuned free-interface natural frequencies of the blades were then extracted through modal analyses performed on each perturbed blade model. From these results, the perturbation coefficients required by the reduced-order formulation were computed using Eq. (21). The mistuned reduced-order model was then constructed by introducing these coefficients into the diagonal block $\boldsymbol{\Omega}_f^2$ of the reduced stiffness matrix of the blade component (see Eq. (20)).

To assess the robustness of the proposed approach, multiple mistuning patterns were considered by varying the standard deviation of the Young's modulus distribution, with values ranging from 5% to 50%. Validation of the reduced-order model was carried out by comparing the natural frequencies of the first 100 modes with those obtained from the FE model of the mistuned 18-blade disk assembly. The comparison between the FEM mistuned model and the proposed mistuned ROM demonstrates very good agreement across all tested mistuning levels (Figure 4).

For small mistuning levels (5% and 10% STD), the deviation between ROM and FEM frequencies is almost negligible, with mean errors below 0.2% and peak errors limited to about 1%. As the mistuning intensity increases (30% and 50% STD), the frequency deviations naturally become more pronounced, but the ROM still retains strong accuracy. Even at the highest mistuning level of 50% STD, the mean error remains below 1%, while the peak error does not exceed 4.3% (Table 1).

**Table 1** Mean and peak errors in natural frequencies of the reduced-order model compared to the full FEM model under different mistuning levels

| | *5 % STD* | *10 % STD* | *30 % STD* | *50 % STD* |
|---|---|---|---|---|
| *Mean error [%]* | 0.12 | 0.19 | 0.39 | 0.98 |
| *Peak error [%]* | 1 | 1 | 1.8 | 4.3 |

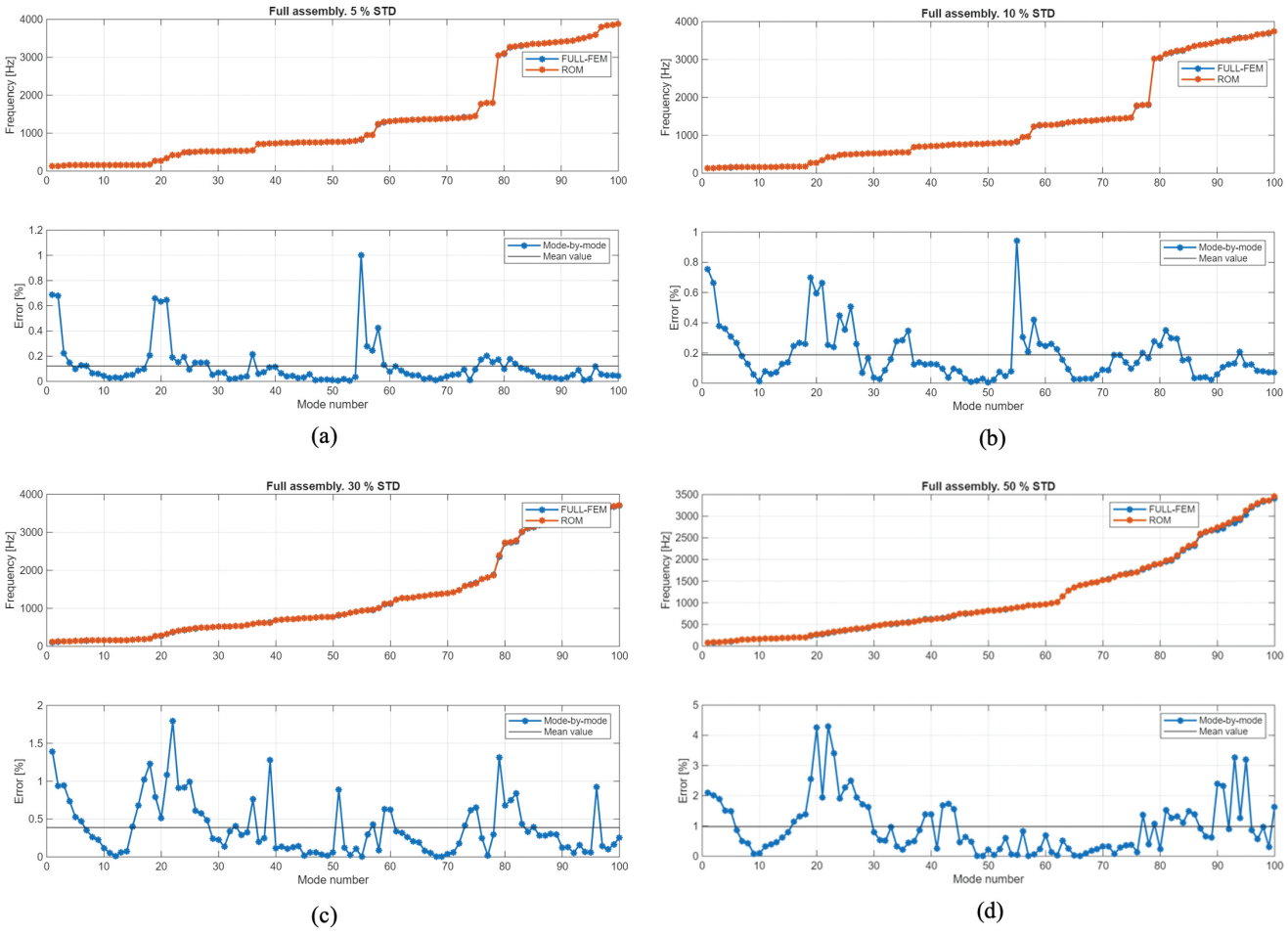


**Fig. 4** Comparison of natural frequencies of the first 100 modes between the full FEM mistuned model and the mistuned reduced-order model (ROM) under different mistuning levels: (a) 5% STD, (b) 10% STD, (c) 30% STD, and (d) 50% STD. The lower plots show the corresponding mode-by-mode frequency errors and mean error values

A key feature observed in the mode-by-mode error plots is that the deviations are not uniformly distributed across modes: certain modes are more sensitive to mistuning, leading to localized peaks in error. Nevertheless, the overall error trend remains very low and well within acceptable bounds for reduced-order modeling. These results confirm that the proposed ROM formulation is not only simple and computationally efficient but also robust to large mistuning levels. The method captures the essential dynamic characteristics of the mistuned bladed disk, providing a reliable alternative to full FEM analysis.

## Conclusion

This paper presents a novel reduction method for mistuned bladed disks, referred to as the Free-Interface Blade Mistuning (FIBM) method. The core innovation of the approach lies in the reduced representation of the blade component using the Rubin reduction method, which allows mistuning to be introduced directly through perturbations of the free-interface natural frequencies. These frequencies retain a clear physical meaning and are independent of the choice of boundary (master) DOFs, enabling a more realistic and experimentally replicable representation of the blade dynamics. This feature addresses a key limitation of Craig–Bampton-based reduced-order models, which do not allow a precise control over the natural frequencies of the free blade, as these are intrinsically altered by the interface constraints applied during reduction.

The proposed method offers several advantages. It enables individual mistuning of each blade and of each associated natural frequency, allowing for the flexible and detailed construction of arbitrary mistuning patterns. Furthermore, the technique is simple to implement, physically interpretable, and robust across a wide range of mistuning intensities,

making it suitable for both academic investigations and practical applications in turbomachinery design and diagnostics.

Validation against a full finite element model of the 18-sector bladed disk demonstrated excellent agreement: the mean error across the first 100 natural frequencies remained below 1.5%, even under strong mistuning conditions, while peak errors stayed within acceptable limits. These results confirm that the proposed reduced-order model (ROM) achieves high predictive accuracy at a significantly lower computational cost.

Future research will focus on the experimental validation of the method using real bladed disk assemblies. Such studies would offer direct evidence of the model's predictive capability under practical conditions, accounting for typical uncertainties such as manufacturing tolerances, material inhomogeneities, and interface boundary variability. Experimental modal analysis would also provide a valuable benchmark to assess the accuracy of the frequency perturbation strategy when compared with measured modal data.

## References


1. Dye, R. C. F., and Henry, T. A., "Vibration Amplitudes of Compressor Blades Resulting from Scatter in Blade Natural Frequencies," ASME Journal of Engineering for Power, Vol. 91, No. 3, pp. 182–188, 1969.
2. Ewins, D. J., "The Effects of Detuning Upon the Forced Vibrations of Bladed Disks," Journal of Sound and Vibration, Vol. 9, No. 1, pp. 65–79, 1969.
3. Griffin, J. H., and Hoosac, T. M., "Model Development and Statistical Investigation of Turbine Blade Mistuning," ASME Journal of Vibration, Acoustics, Stress, and Reliability in Design, Vol. 109, pp. 204–210, 1984.
4. Yang, M.-T., and Griffin, J. H., "A Reduced Order Model of Mistuning Using a Subset of Nominal Modes," ASME Paper 99-GT-288, International Gas Turbine Institute Turbo Expo, Indianapolis, IN, 1999.
5. Bladh, R., Castanier, M. P., and Pierre, C., "Component-Mode-Based Reduced Order Modeling Techniques for Mistuned Bladed Disks—Part I: Theoretical Models," ASME Journal of Engineering for Gas Turbines and Power, Vol. 123, No. 1, pp. 89–99, 2001.
6. Bladh, R., Castanier, M. P., and Pierre, C., "Component-Mode-Based Reduced Order Modeling Techniques for Mistuned Bladed Disks—Part II: Application," Proceedings of the ASME Turbo Expo 2000: Power for Land, Sea, and Air, Vol. 4, Munich, Germany, May 8–11, 2000.
7. Feiner, D. M., and Griffin, J. H., "A Fundamental Model of Mistuning for a Single Family of Modes," ASME Journal of Turbomachinery, Vol. 124, No. 4, pp. 597–605, 2002.
8. Vargiu, P., Firrone, C. M., Zucca, S., and Gola, M. M., "A Reduced Order Model Based on Sector Mistuning for the Dynamic Analysis of Mistuned Bladed Disks," International Journal of Mechanical Sciences, Vol. 53, No. 8, pp. 639–646, 2011.
9. Pourkiaee, M. S., and Zucca, S., "A Reduced Order Model for Nonlinear Dynamics of Mistuned Bladed Disks With Shroud Friction Contacts," ASME Journal of Engineering for Gas Turbines and Power, Vol. 141, No. 1, pp. 011031, 2019.
10. Saletti, G., Pourkiaee, M., and Zucca, S., "Mass Mistuning Reduced Order Models for Bladed Disks With Shroud Friction Joints," Proceedings of the ASME Turbo Expo 2024: Turbomachinery Technical Conference and Exposition, Vol. 10B, London, United Kingdom, June 24–28, 2024.
11. Rubin, S., "Improved Component-Mode Representation for Structural Dynamic Analysis," AIAA Journal, Vol. 13, pp. 995–1006, 1975.
12. Craig, R., and Bampton, M., "Coupling of Substructures for Dynamic Analysis," AIAA Journal, Vol. 6, pp. 1313–1319, 1968.
13. Battiato, G., Firrone, C. M., Berruti, T. M., and Epureanu, B. I., "A General Method for Sub-Systems Coupling for the Dynamic Analysis," Proceedings of the ISMA Conference, Leuven, Belgium, 2016.
14. Castanier, M. P., Tan, Y.-C., and Pierre, C., "Characteristic Constraint Modes for Component Mode Synthesis," AIAA Journal, Vol. 36, No. 6, pp. 1182–1187, 2001.
15. Craig, R. R., and Kurdila, A. J., Fundamentals of Structural Dynamics, 2nd ed., Wiley, Hoboken, NJ, 2006.
16. Battiato, G., Vibrations Prediction and Measurement of Multi-Stage Bladed Disks with Nonlinear Behavior due to Friction Contacts, Ph.D. Dissertation, Politecnico di Torino, Turin, Italy, 2017.
17. Battiato, G., and Firrone, C. M., "Reduced Order Modeling of Large Contact Interfaces to Calculate the Non-Linear Response of Frictionally Damped Structures," Procedia Struct. Integr., 24, pp. 837–851, 2019
18. Battiato, G., and Firrone, C. M., "A Modal Based Reduction Technique for Wide Loose Interfaces and Application to a Turbine Stator," Mech. Syst. Signal Process., 139, p. 106415, 2020.
19. Allen, M. S., Rixen, D., van der Seijs, M., Tiso, P., Abrahamsson, T., and Mayes, R. L., Substructuring in Engineering Dynamics: Emerging Numerical and Experimental Techniques, CISM International Centre for Mechanical Sciences, Vol. 2020, Springer Cham, 2020.